Ocean Engineering 159 (2018) 22–36

Contents lists available at ScienceDirect

Ocean Engineering

journal homepage: www.elsevier.com/locate/oceaneng

Extreme value analysis of wave climate in Chesapeake Bay

Arash Niroomandi [a], Gangfeng Ma [a,*], Xinyu Ye [b], Sha Lou [c], Pengfei Xue [b]

[a] Department of Civil and Environmental Engineering, Old Dominion University, Norfolk, 23455, VA, USA
[b] Department of Civil and Environmental Engineering, Michigan Technological University, Houghton, 49931, MI, USA
[c] Department of Hydraulic Engineering, Tongji University, Shanghai, 200092, China

ARTICLE INFO

Keywords:
Chesapeake bay
Design wave height
Generalized extreme value distribution
Generalized Pareto distribution
Empirical orthogonal function

ABSTRACT

A thirty-seven year wave hindcast (1979–2015) in Chesapeake bay using NCEP's Climate Forecast System Reanalysis (CFSR) wind is presented. The long-term significant wave heights are generated by the third-generation nearshore wave model SWAN, which is validated using the wave height measurements at buoy stations in the bay. The simulated wave heights are analyzed to characterize their temporal and spatial variabilities as well as long-term changing trends by using an Empirical Orthogonal Function (EOF) analysis and an empirical cumulative distribution function approach. Seasonal variability as well as extreme storm effects on significant wave heights are revealed in the first mode of principle component. Then, an extreme value analysis based on generalized extreme value and generalized Pareto distribution functions is applied to evaluate design wave heights with different return periods. The effects of key parameters including threshold value, time span and data length on the design wave heights are extensively studied. Through the comparisons of different distribution functions evaluated by Bayesian Information Criterion and Akaike Information Criterion, it is found that Gamma distribution function and generalized extreme value analysis provide the best fit for annual and monthly data, while generalized Pareto distribution function gives the best fit when peak-over-threshold analysis is conducted.

1. Introduction

Coastal planners and engineers increasingly require information about wave climate to make better planning decisions and minimize future coastal hazards and economic loss, because coastal waves play a significant role in coastal flooding and damage of coastal infrastructure. Wave studies in the field of ocean and coastal engineering have usually focused on characterizing the spatial and temporal variabilities of characteristic wave height, typically the significant wave height, and determining the design wave heights for structure design purposes.

To study spatial and temporal variabilities of significant wave height, statistical analysis of long-term wave climate data could be performed. For example, Empirical Orthogonal Function (EOF) analysis provides useful information regarding possible spatial patterns of variability within the data and how they change with time. EOF analysis has been widely used in oceanography to study major modes of climate variability such as the El Nino/Southern Oscillation (ENSO) (Roundy, 2015; Lian and Chen, 2012; Messie and Chavez, 2011), and in coastal engineering to identify spreading and seasonal variability in shoreline and slope data (Lemke and Miller, 2017). The long-term changing trends of wave height can be revealed by means of a regression analysis and an empirical cumulative distribution function approach, which have been applied in a number of recent studies on extreme wave height in different ocean and coastal regions (Komar and Allan, 2007, 2008; Ruggiero et al., 2010). Long-term trend of extreme wave height is of considerable interest in recent wave studies because significant changes in wave heights have been found in many coastal and ocean regions. For instance, Mendez et al. (2006) and Menendez et al. (2008) revealed significant long-term variability of extreme wave height in the Northeast Pacific ocean using buoy measurements and a time-dependent peak over threshold (POT) model. In the North Atlantic ocean near the coast of England (Carter and Draper, 1988; Bacon and Carter, 1991) and east coast of U.S. (Komar and Allan, 2007, 2008), researchers have found significant increases in wave height generated by extreme storms during the past decades. Similar results have also been reported in other locations such as west coast of U.S. using measurements from NOAA buoy stations (Komar et al., 2009; Allan and Komar, 2000; 2006; Ruggiero et al., 2010) and by analysis of storm intensities and hindcasted wave heights (Graham and Diaz, 2001).

To determine the design wave heights, extreme value analysis of significant wave height is always performed. Extreme value analysis (EVA) has broad applications in many disciplines such as coastal engineering, weather and climate, finance and traffic prediction. The theory

* Corresponding author.
E-mail address: gma@odu.edu (G. Ma).

https://doi.org/10.1016/j.oceaneng.2018.03.094
Received 17 November 2017; Received in revised form 29 March 2018; Accepted 31 March 2018

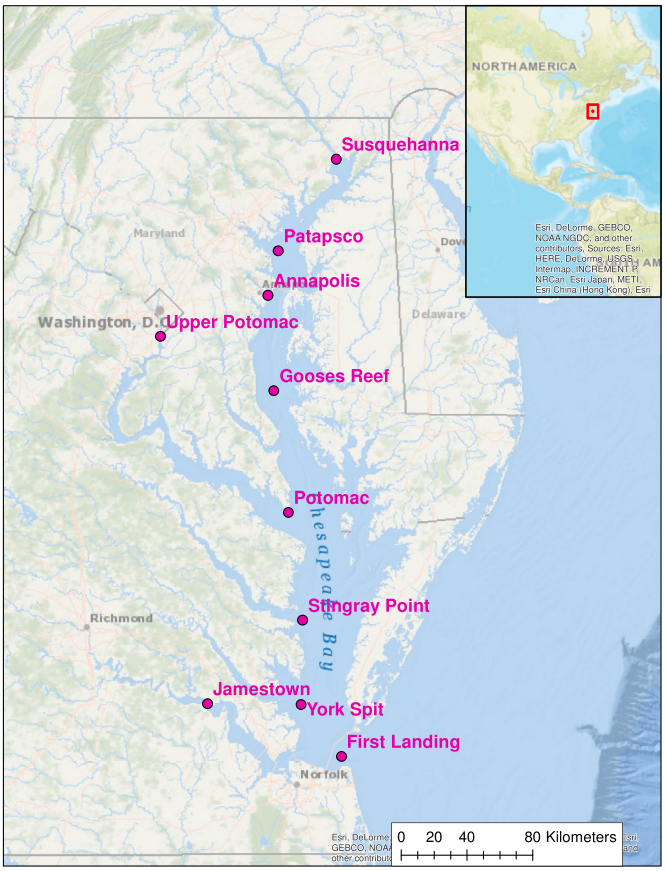

Fig. 1. Chesapeake Bay and location of Buoys inside the Bay.

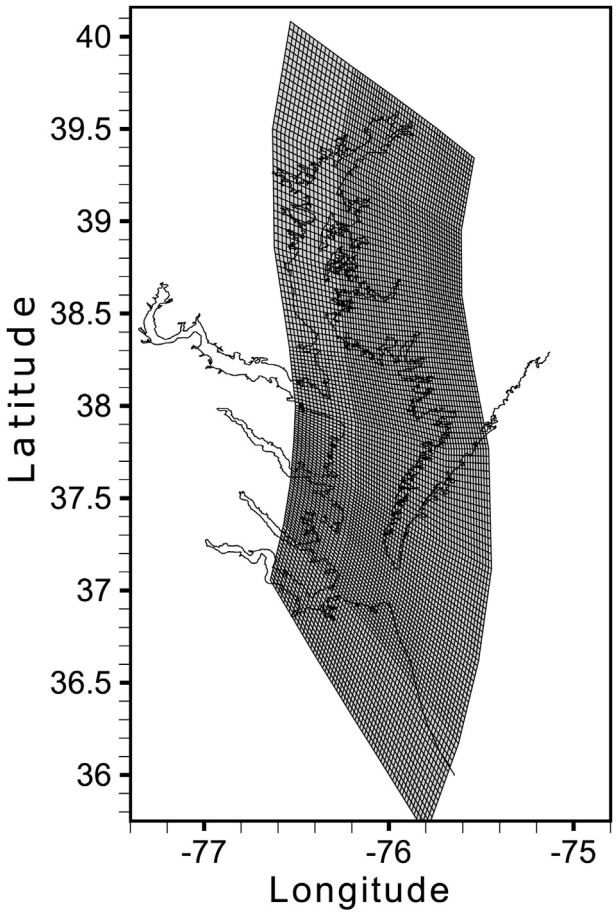

Fig. 2. The computational grid for SWAN wave model.

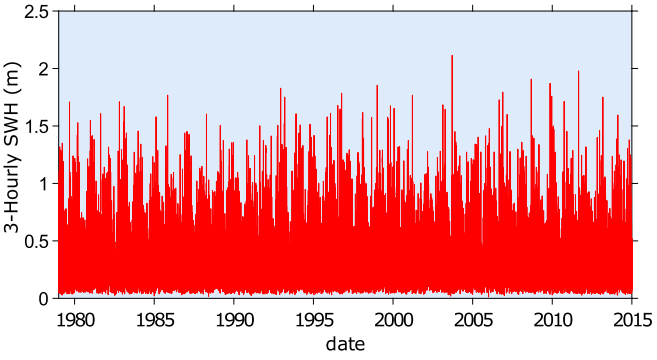

Fig. 3. The simulated 3-Hourly significant wave height (SWH) at Stingray Point in Chesapeake Bay during 1979 2015.

of EVA has been presented by a number of researchers (Gumbel, 2012; Coles et al., 2001; Kotz and Nadarajah, 2000; Katz et al., 2002; Hawkes et al., 2008; Cooley, 2009, 2013; Cooley et al., 2007). Its applications on extreme wave height analysis were presented by Goda (1992), Mathiesen et al. (1994) and Menendez et al. (2008). The central idea of extreme wave height analysis is to determine the long-term variability of significant wave height through implementations of distribution functions and quantile functions as well as extrapolation of historical data (Goda, 1992; Muir and El-Shaarawi, 1986; Muraleedharan et al., 2012). The unknown parameters of the distribution functions are determined by a fitting method. The common fitting methods include maximum likelihood estimate (MLE), generalized maximum likelihood estimate (GMLE), the method of moments (MOM), probability weighted moment (PWM), least square method (LSM), Bayesian and L-moments (Coles et al., 2001). Each of these methods has its own merits and demerits. For example, for small sample data, MLE might not give good estimate of parameters and L-moment could be used instead. MOM quantile estimators have smaller root mean square errors for specific range of shape parameter values than L-moment and MLE (Martins et al., 2000). More detailed information regarding the estimators can be referred to Martins et al. (2000). After the determinations of distribution functions and quantile functions, the extreme wave height data is organized in a way that is feasible for extrapolation. The design wave heights can be finally determined given different return periods and probabilities of occurrence.

This paper is dedicated to investigating wave climate in Chesapeake Bay. Due to the lack of reliable long-term wave data, limited studies on wave climate in Chesapeake bay have been carried out. However, significant advances in satellite altimeters have made it possible for researchers to use wave models to reproduce the historical wave height using reanalysis technique. This technique has been utilized in many earlier studies on wave climate analysis, for example, Stopa et al. (2013), Stopa and Cheung (2014), Chawla et al. (2013), Rascle and Ardhuin (2013), Tolman et al. (2013), Mentaschi et al. (2015), Anderson et al. (2015). In this study, the third-generation nearshore wave model SWAN is applied to reconstruct long-term significant wave height in the entire Chesapeake Bay. The objectives of this study are (1) to hindcast significant wave height in the bay during 1979–2015; (2) to investigate spatial and temporal variabilities of significant wave height in the bay; (3) to determine and compare design wave heights by extreme value analysis.

The paper is organized as follows. The data and methodology are introduced in section 2. In section 3, the simulated significant wave heights are analyzed statistically to reveal their spatial and temporal variabilities in the past decades. Extreme value analysis of the significant wave heights are presented in section 4. Sensitivity of extreme wave

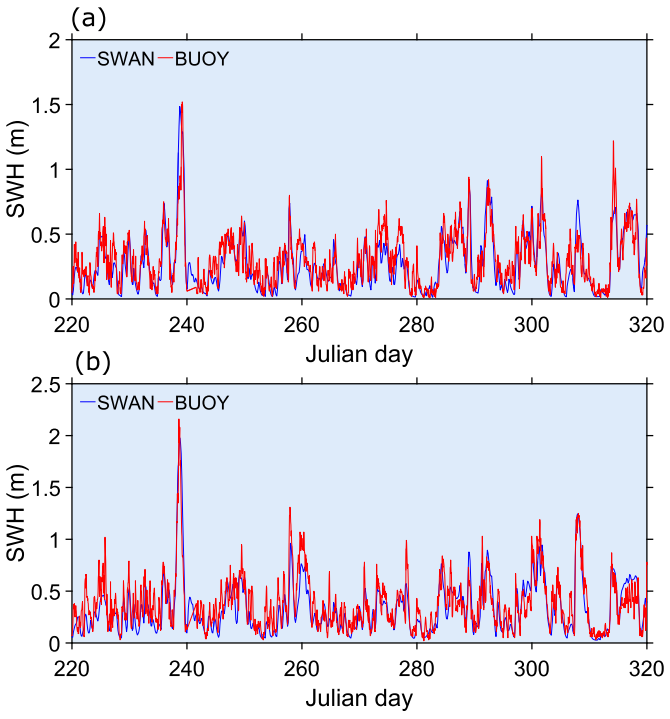

Fig. 4. Comparisons between simulations and measurements for a selected time period in year 2011 at (a) Potomac (b) Stingray Point.

height analysis to key parameters is discussed in section 5 and finally conclusions are presented in section 6.

2. Wave model

Although understanding of wave characteristics is essential in many aspects including navigational and design purposes, this knowledge has been limited in Chesapeake Bay mostly because of scarcity of reliable observational data (Farnsworth, 1997). Recently, a number of buoy systems were deployed by the National Oceanic and Atmospheric Administrations (NOAA) Chesapeake Bay Interpretive Buoy System (CBIBS) to gather meteorological, oceanographic, and water-quality data. The program was launched in 2007 and the total number of buoys deployed so far is ten. The locations of these buoys are shown in Fig. 1. These buoys are capable of collecting information on a variety of parameters including significant wave height and period, maximum wave height and mean wave direction. Data is collected every 10–60 min depending on the parameter and is accessible through their website (http://buoybay.noaa.gov). CBIBS provide valuable short-term wave height data for wave model validation.

To hindcast long-term significant wave height in Chesapeake bay, 37 years wind data (1979–2015) were collected through the National Centers for Environmental Prediction (NCEP) Climate Forecast System Reanalysis (CFSR) (Saha et al., 2010, 2014). The CFSR uses a coupled atmosphere-ocean-land surface-sea ice system with advanced data assimilation techniques and an extensive database of meteorological observations to create its products. The original CFSR dataset spans from 1979 to 2010 and the second version of the Climate Forecast System (CFSv2) provides products from 2011 up until now with several improvements over CFSR, such as a higher spatial resolution (Saha et al., 2014). Temporal resolution for both models is 6 h. However, spatial resolution of the CFSv2 is approximately 20 km compared to 38 km for CFSR, which is a significant improvement. In this study, the third-generation SWAN wave model (Rusu et al., 2009) is employed to obtain 3-hourly significant wave heights for the past 37 years. The computational domain encompasses the full Chesapeake Bay and a

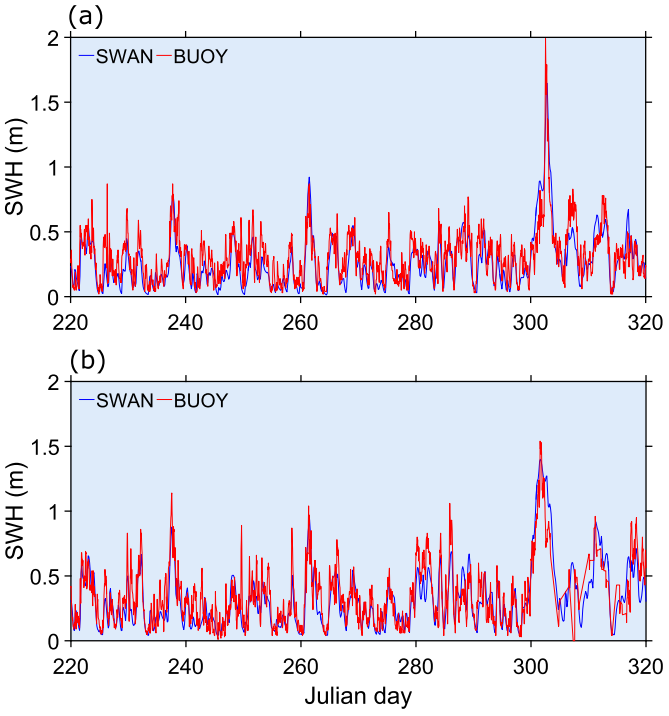

Fig. 6. Comparisons between simulations and measurements for a selected time period in year 2012 at (a) Potomac (b) Stingray Point.

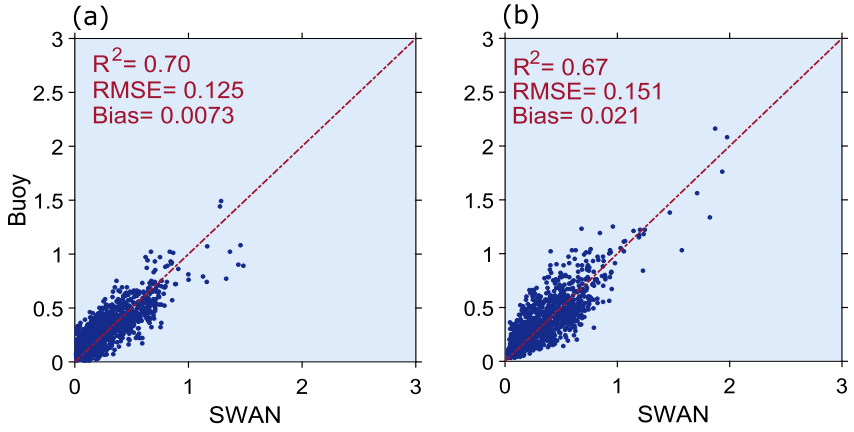

Fig. 5. Correlations between simulations and measurements for a selected time period in year 2011 at (a) Potomac (b) Stingray Point.

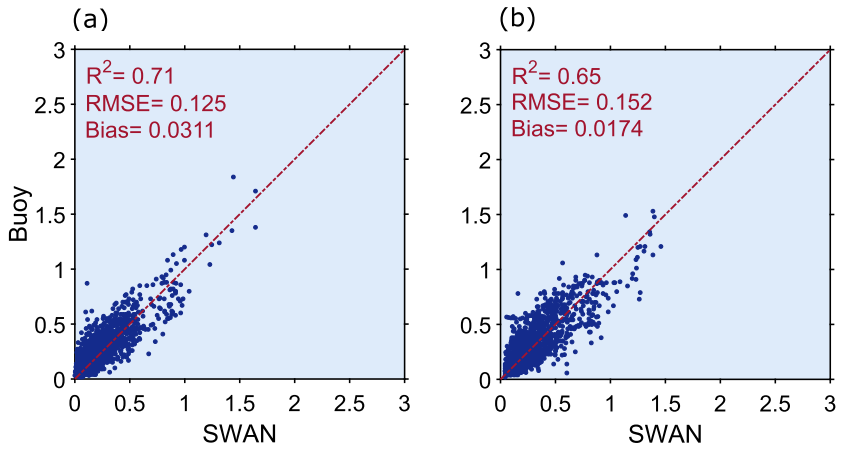

Fig. 7. Correlations between simulations and measurements for a selected time period in year 2012 at (a) Potomac (b) Stingray Point.

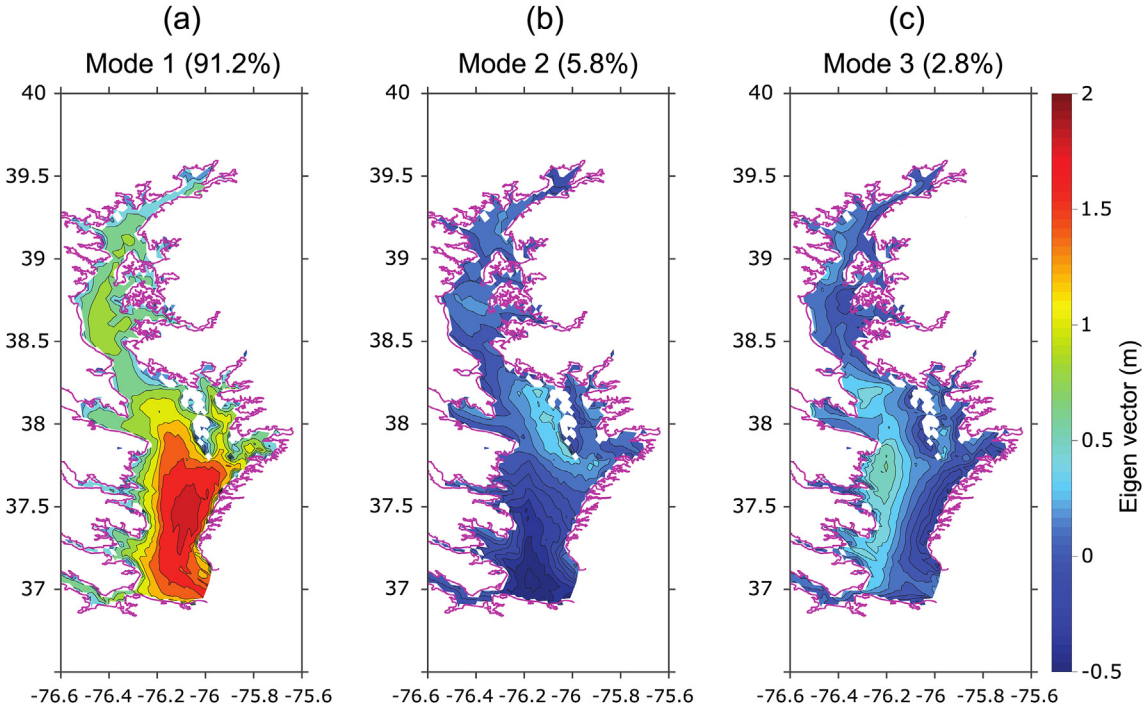

Fig. 8. EOF analysis of daily-averaged SWHs and extraction of dominant modes of spatial variability (a) mode 1 (b) mode 2 (c) mode 3. Mode 1 accounts for more than 90% of spatial variability.

portion of the nearby coastal region. The computational grid is curvilinear and includes 129 × 65 mesh cells (Fig. 2). The bathymetry data is from NCEI Estuarine Bathymetric Digital Elevation model. For the SWAN simulations, wave energy dissipation mechanisms including white capping, wave breaking and bottom friction are triggered. As an example, the simulated significant wave heights (SWHs) for 37 years at Stingray Point are depicted in Fig. 3. Seasonal variability of the wave heights can be clearly seen. Because the hindcasted wave height data set is huge, the model-data comparisons in selected time periods are shown in order to demonstrate the model performance. The simulated and measured SWHs at buoy stations Potomac and Stingray Point in year 2011 and 2012 are compared in Figs. 4 and 6. The reason of choosing year 2012 for demonstration is because wave climate in Chesapeake bay was affected by hurricane Sandy in this year. It can be seen that the simulations match reasonably well with the measurements. Particularly, the wave height variations during hurricane Sandy were captured by the model. To quantify the model performance, the correlations between simulations and measurements at Potomac and Stingray Point during 2011 and 2012 are presented in Figs. 5 and 7. Particularly, the bias $= \frac{1}{N}\sum_{i=1}^{N}(M_i - O_i)$, RMSE and correlation coefficients are evaluated and shown in the figures. The coefficients of determination (R^2) are above 0.62 and the bias and RMSE are reasonably small, indicating that the SWAN model is capable of simulating temporal variations of SWHs with reasonable accuracy.

3. Spatial and temporal variabilities of SWHs

The reconstructed SWHs exhibit temporal and spatial variabilities. In order to reveal their patterns, an empirical orthogonal function (EOF) analysis on daily-averaged SWHs is performed. Like Fourier analysis, the EOF provides an expansion of the original data in a series of functions that separate the spatial and temporal variations. These functions are determined by the correlations within the data set and may suggest certain processes or time scales of change. The idea of EOF analysis is to

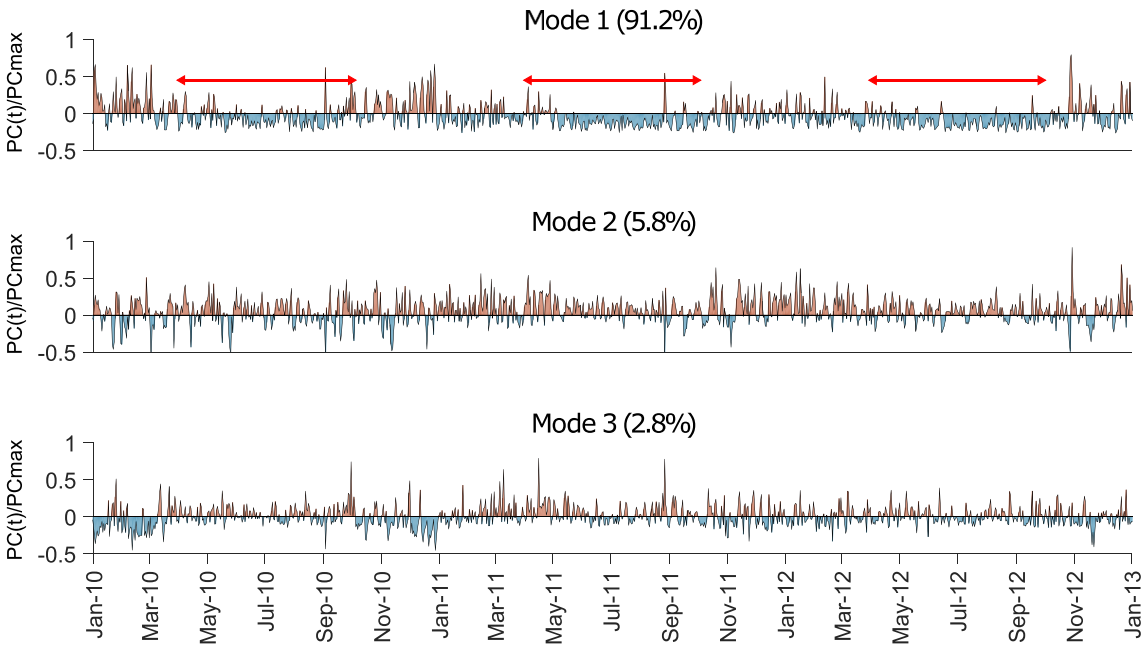

Fig. 9. EOF analysis of daily-averaged SWHs and extraction of dominant modes of temporal variability (a) mode 1 (b) mode 2 (c) mode 3. Seasonal variability of SWHs is observed from Mode 1. Non-winter seasons are shown using red arrow. (For interpretation of the references to colour in this figure legend, the reader is referred to the Web version of this article.)

Table 1
Name and occurrence time of hurricanes and tropical storms inside Chesapeake Bay for the past decade.

Name	Date
Hurricane Sandy	Oct. 26, 2012
Hurricane Irene	Aug. 26–28, 2011
Hurricane Ida	Nov. 10–14, 2009
Hurricane Hanna	Sep. 6, 2008

express the time series data as

$$Z(x,y,t) = \sum_{k=1}^{N} PC(t)\cdot EOF(x,y) \tag{1}$$

where $Z(x,y,t)$ is the original time series as a function of time (t) and space (x,y), $EOF(x,y)$ is the eigenfunctions (or vectors) of the correlation matrix of the data, which shows the spatial structures of the major factors that account for the spatial variations of the data, and PC(t) is the principal component describing the temporal variation of each EOF. The EOFs can be obtained by computing the eigenvalues and eigenvectors of a spatially weighted anomaly covariance matrix of a field and the resulting eigenvalues provide a measure of the percentage variance explained by each mode. The lower-mode EOFs represent large-scale variability and higher-mode EOFs show smaller scales or even sometimes random noises. In this study, EOF analysis is performed using a Matlab package and results for the first three modes are presented in Figs. 8 and 9, respectively.

Fig. 8 demonstrates the spatial distributions of the first three dominant EOF modes for the entire Chesapeake bay. The corresponding PCs are presented in Fig. 9, in which the values are scaled to the range between −1 and 1 by dividing their maximum values. From the calculated eigenvalues, it can be determined that the mode 1 accounts for 91.2% of spatial variability of SWHs. The other modes only contribute to a small part of the signal variance. Clearly, the PC of mode 1 demonstrates a seasonal variability of SWHs, with positive PC in winter season (October–March) and negative PC in summer season. The first EOF mode describes deviation from the mean SWH. Combined with the first PC mode, it can be interpreted that, in winter season when PC is positive, the wave heights are generally greater than the mean SWH. While in summer season when PC is negative, the wave heights are generally smaller than the mean SWH. The seasonal variation of wave climate is typical in coastal regions. From Fig. 8, it is also found that the first EOF has the largest value in the lower Chesapeake bay and the smallest value in the upper bay. It is because the lower bay is more exposed and wave height variations are more significant in this region. Since the other PC modes do not show clear variation patterns, they are not discussed herein.

In the first PC mode in Fig. 9, several spikes with large positive PC values can be detected. These anomalies are generally linked with hurricane or tropical storm events. Table 1 shows the names of tropical storms and times of occurrence in the past decade. Largest PC values are spotted when storms hit the bay as shown in Fig. 10. There is a close correlation between occurrence of storms and mode 1 eigenvalues.

The changing trend of significant wave height at a representative site is analyzed using a regression analysis. Stingray Point is selected for this purpose since this point is not far from the mouth of the bay so it can capture extreme wave heights entering the bay. Regression analysis is performed on winter-averaged and annual maxima data derived from SWAN results, which are depicted in Fig. 11a. It is found that extreme wave heights at this station were generally increasing. The increasing rate of annual maximum wave heights is much higher than that of winter average (4.1 mm/yr versus 1.4 mm/yr).

To examine the robustness of the regression analysis, sensitivity of the calculated trends are tested with respect to the amount of data included in the analysis. Regression analysis is firstly performed using data from 1979 to 2008, and then rate of increase is computed by adding data annually. This process is repeated until all years are included in the analysis. The computed increasing rates for annual maxima and winter average are presented in Fig. 11b. Results show that except year 2011 in which there is a decrease in winter average and a sudden increase in annual maxima, rates of wave height increase are fairly stable regardless of the amount of data used. The decrease in winter average and increase in annual maxima in 2011 can be associated with hurricane Irene which passed through Chesapeake Bay in August.

Statistical significance test has been used widely in hydrology and coastal engineering (Tasdighi et al., 2017; Ruggiero et al., 2010) to

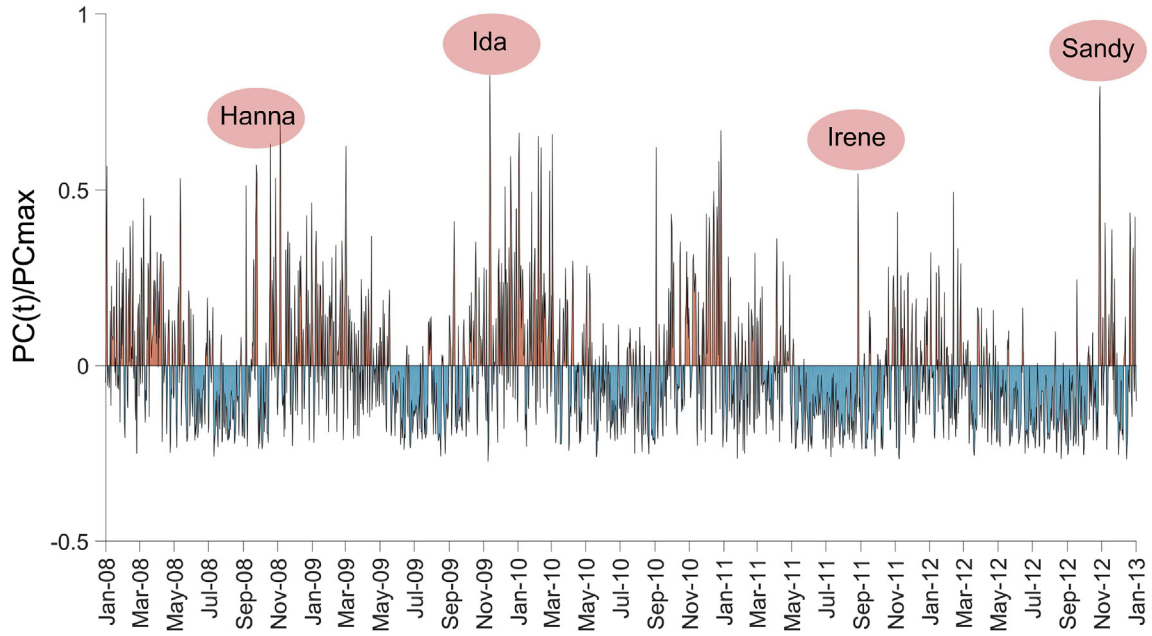

Fig. 10. Detection of significant storm events in Chesapeake Bay by EOF analysis.

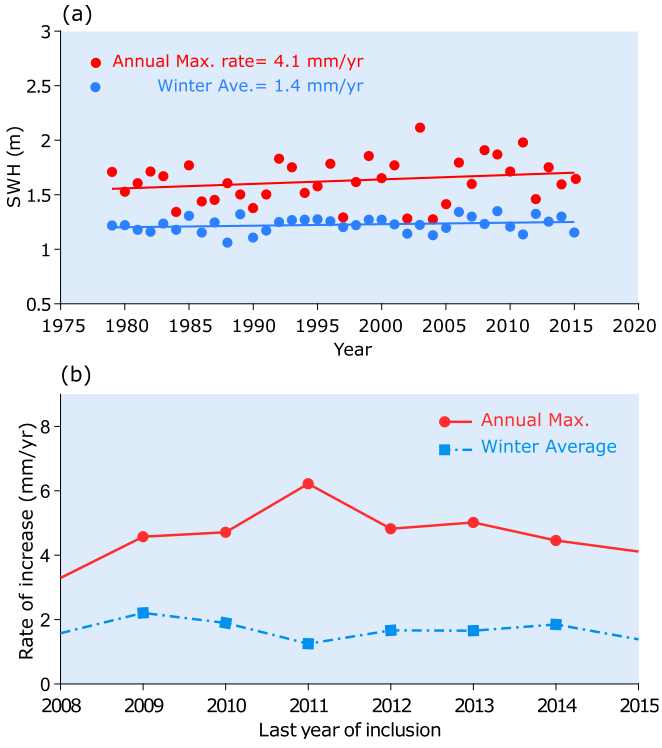

Fig. 11. (a) Decadal increases in winter average and annual maxima SWHs (b) Rate of increase of the winter average and annual maxima SWHs at Stingray Point.

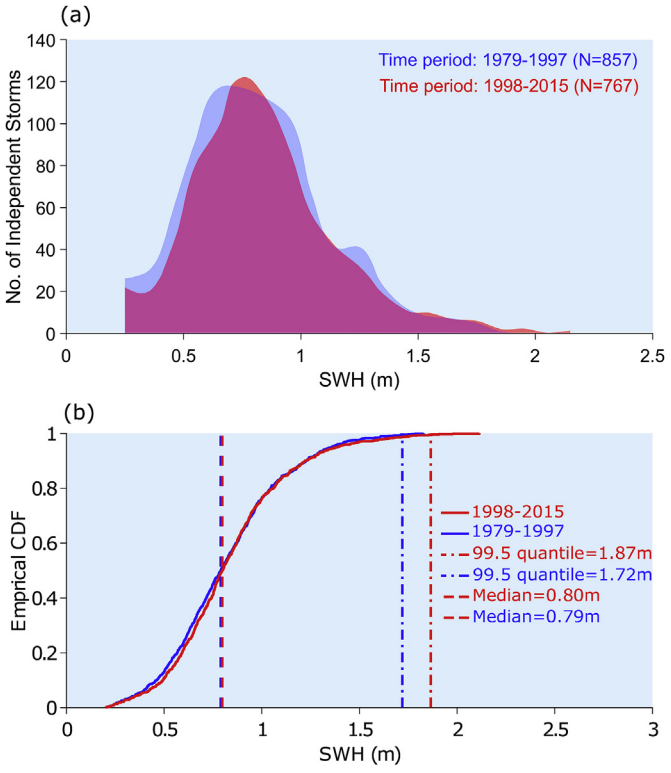

Fig. 12. Comparison of the numbers of independent storms for the periods 1979–1997 and 1998–2015, documenting the shift in the wave climate to higher waves (a) number of distributions for a range of SWHs (b) empirical cumulative distribution functions. The analyses are based on the simulated SWHs at Stingray Point.

examine the significance of the slope of a regression model. In this study, the statistical significance test is performed on each subset of data to examine whether or not the rates of SWH increases derived from regression analysis are statistically significant. The significance test results in a p-value > 0.05, meaning that for both winter average and annual maxima, rate of increases are not statistically significant.

In order to further examine the progressive increases of waves, more detailed analysis of SWHs is provided using probability distributions of all independent storms. Independent storm is defined by Mendez et al. (2006). In this definition, minimum time span between 2 consecutive storms should be selected such that Poisson process is assumed to be valid. Fig. 12a shows the number of independent storms occurred for a range of SWHs during two time periods: The first period is defined from

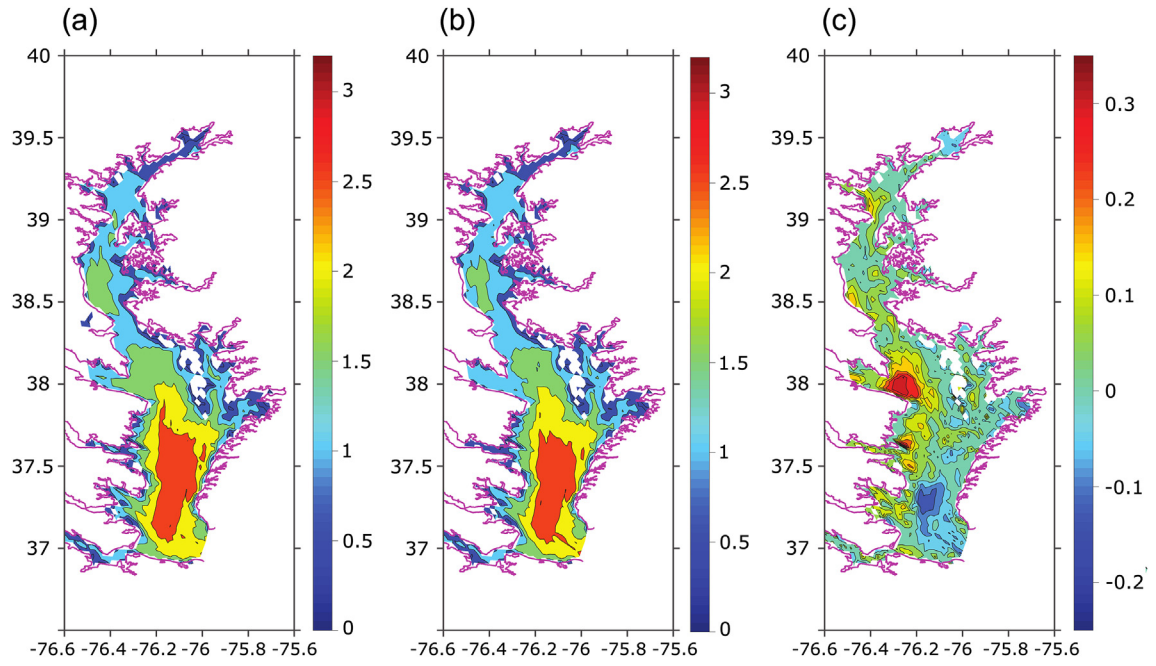

Fig. 13. 99.5 percentile of independent storms (in meters) during periods (a) 1979–1997 (b) 1998–2015 (c) difference of two periods. Results show that the bay experiences a slight increase in extreme wave heights except the lower bay.

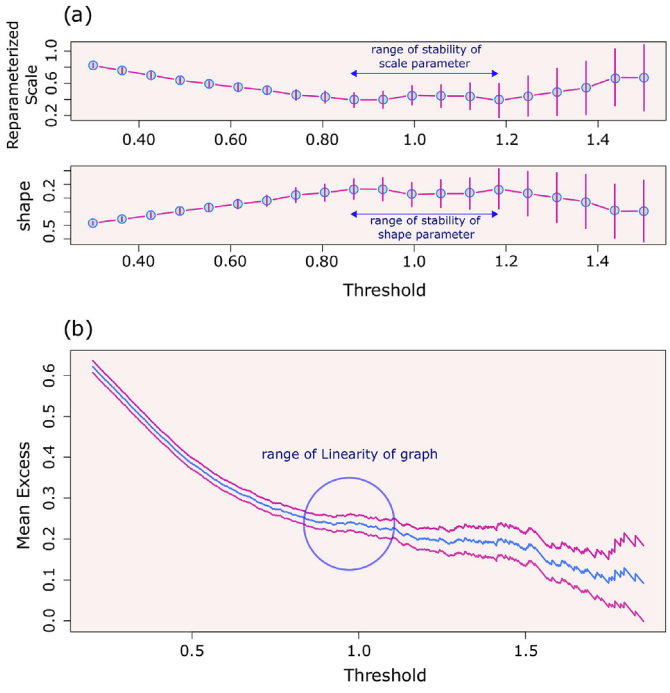

Fig. 14. Threshold selection using (a) parameter stability plot and (b) mean residual life plot.

1979 to 1997 and the second one is from 1998 to 2015. Results show that although total number of independent storms are higher during 1979–1997 by about 12%, the number of extreme storms with SWH larger than 1.5m exceeds by 33% during period 1998–2015. More explicit explanation of progressive increases of extreme storms is presented in Fig. 12b in which the empirical cumulative distribution functions for the two periods are depicted. Although medians for the two periods are almost the same (0.79m and 0.80m for periods 1979–1997 and 1998–2015, respectively), a 9% increase is observed in 99.5 percentile in the period of 1998–2015, confirming the findings from the regression analysis presented in Fig. 11 and demonstrating a slight shift towards higher values of extreme wave heights in the past decades. It is also shown that there is a consistency between the annual increasing rates of SWHs based on regression analysis and cumulative distribution function analysis.

A more comprehensive study of progressive increases of waves in Chesapeake bay is performed by obtaining 99.5 percentile of independent storms during periods 1979–1997 and 1998–2015 for the entire bay, which are presented in Fig. 13. Except lower bay where a maximum decrease of 0.27m in extreme wave height is observed (Fig. 13c), the rest of the bay experiences an average increase of 0.1 m and the maximum increase is found to be 0.36 m in the central bay. Although these changes are small in terms of intensity, they confirm a slight increase in wave heights during the past decades.

4. Extreme value analysis

In this section, extreme value analysis will be performed to obtain design wave heights corresponding to different return periods using various extreme value assessment models, to examine applicability of these models and to perform sensitivity analysis on extracted data to determine the uncertainty that comes along with extreme value models. In extreme value theory, it has been shown that, for sufficiently long sequences of independent and identically distributed random variables, the maxima of samples of size n, can be fitted into the generalize extreme value (GEV) family of distributions, which has the following cumulative distribution function (Coles et al., 2001)

$$G(z,\mu,\sigma,\xi) = \begin{cases} exp\left[-\left(1+\xi\frac{z-\mu}{\sigma}\right)^{-1/\xi}\right], & \xi \neq 0 \\ exp\left[-exp\left(-\frac{z-\mu}{\sigma}\right)\right], & \xi = 0 \end{cases} \quad (2)$$

where μ, σ and ξ are the location, scale and shape parameters, respectively. The three classes of GEV distribution functions are Gumbel distribution (Type I, $\xi = 0$), Frechet distribution (type II, $\xi < 0$) and Weibull distribution (type III, $\xi > 0$). The return level corresponding to return

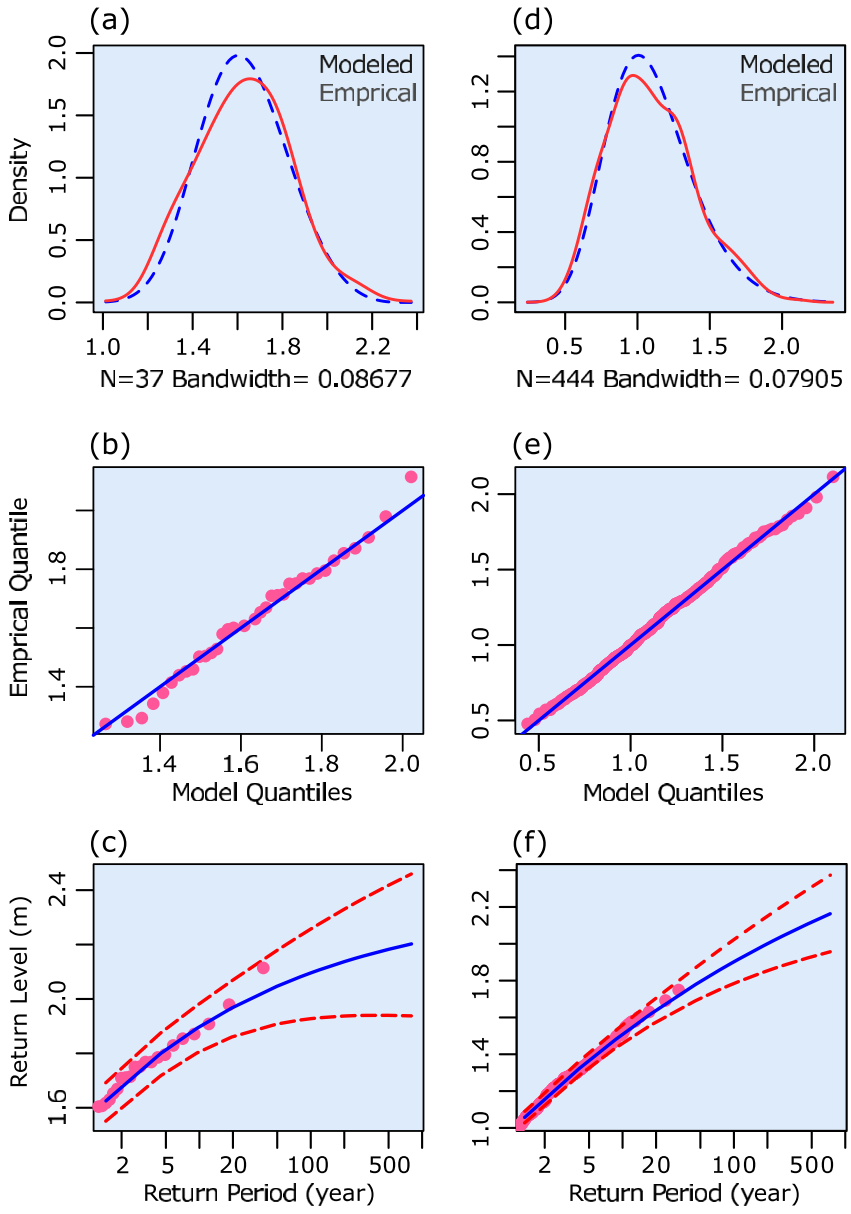

Fig. 15. Diagnostic plots from fitting the GEV df to annual maximum (left panel) and monthly maximum (right panel) SWHs (a,d) Density plots of empirical data and fitted GEV df (b,e) Quantile quantile plot (c,f) Return level plot with 95% confidence intervals.

Table 2
Return levels using annual maxima and different parameter estimation methods.

Return period (year)	Return level (m)	
	LMoments	MLE
10	1.90	1.89
25	1.97	1.98
50	2.04	2.04
100	2.09	2.09

period T can be obtained using the following equation

$$R_T = \begin{cases} \mu - \frac{\sigma}{\xi}\left\{1 - \left[-ln\left(1-\frac{1}{T}\right)^{-\xi}\right]\right\}, & \xi \neq 0 \\ \mu - \sigma ln\left[-ln\left(1-\frac{1}{T}\right)\right], & \xi = 0 \end{cases} \quad (3)$$

One major concern with GEV approach is that GEV is often applied to annual maxima data, hence ignores other significant extreme events in each year. Other approaches that can be used to reduce this limitation are block maxima and peak-over-threshold (POT) method. In block maxima approach, the entire data is divided into non-overlap periods of equal size called block and maximum value in each block is selected for analysis. An example of block maxima approach is monthly maxima which is also included in this study. In the POT method, a high threshold is selected

Table 3
Return levels using monthly maxima and different parameter estimation methods.

Return period (year)	Return level (m)	
	LMoments	MLE
10	1.50	1.50
25	1.68	1.67
50	1.8	1.79
100	1.91	1.90

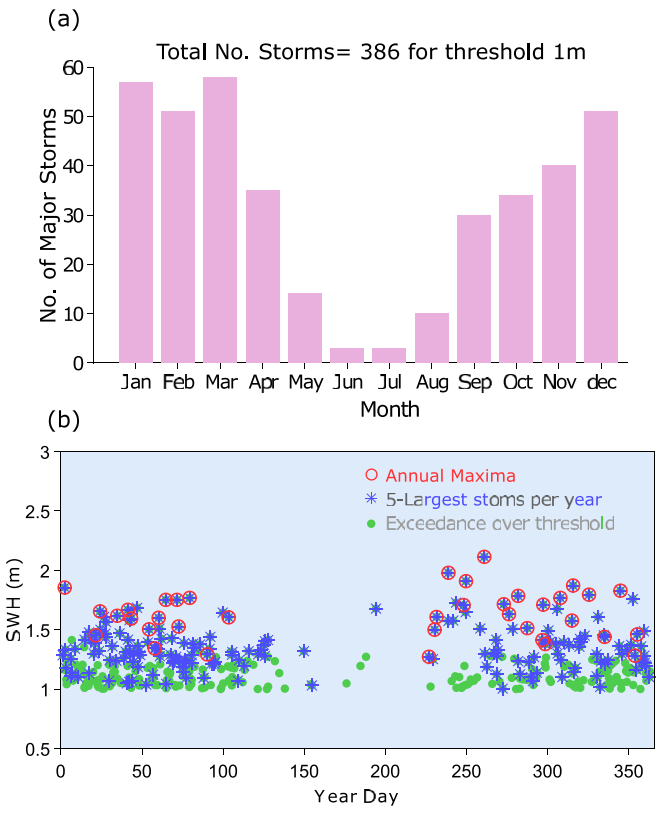

Fig. 16. (a) Number of storm events in which the SWH exceeded a threshold of 1m per calendar month (b) Year day of exceedance above the threshold (dots), annual maxima (circles) and the five largest storms per year (asterisks), indicative of the seasonality of extreme wave heights in Chesapeake Bay. The analysis is based on the simulated SWHs at Stingray Point.

and extreme value analysis is performed on all the data above the given threshold. It can be shown that for sufficiently high threshold, the data can be fitted into the so-called generalized Pareto (GP) distribution function given by

$$F(z,\sigma,\xi) = \begin{cases} 1-\left(1+\xi\frac{z}{\sigma}\right)^{-1/\xi}, & \xi \neq 0 \\ 1-exp\left(-\frac{z}{\sigma}\right), & \xi = 0 \end{cases} \quad (4)$$

where $\sigma > 0$ is the scale parameter and ξ is the shape parameter of the GP distribution function.

Two important concerns with POT approach are the selection of the threshold and the minimum time span Δt, which could affect the results in terms of frequency and exceedance estimates (Mendez et al., 2006). Regarding the time span, Δt should be chosen sufficiently long to guarantee the independency between consecutive storms, and to satisfy the validity of Poisson process. A wide range of Δt can be found in the literature (Luceno et al., 2006; Mendez et al., 2006). In this section, $\Delta t =$ 3 days is selected. Results for $\Delta t = 4, 5$ and 6 days are presented in the discussion section to investigate the sensitivity of time interval on the results.

The choice of threshold is also important in the POT analysis. The threshold (u) should be taken sufficiently high for the distribution function to provide a reasonable estimate. Nevertheless, it cannot be too high to produce large variance on the estimated parameters. Common approaches for selecting threshold include parameter stability plot and mean residual life plot. In the first approach, the parameter estimates from GP distribution function are plotted against a range of values of u. The parameter estimates should be stable above the threshold at which the GP model becomes valid. In the second approach, u is plotted against

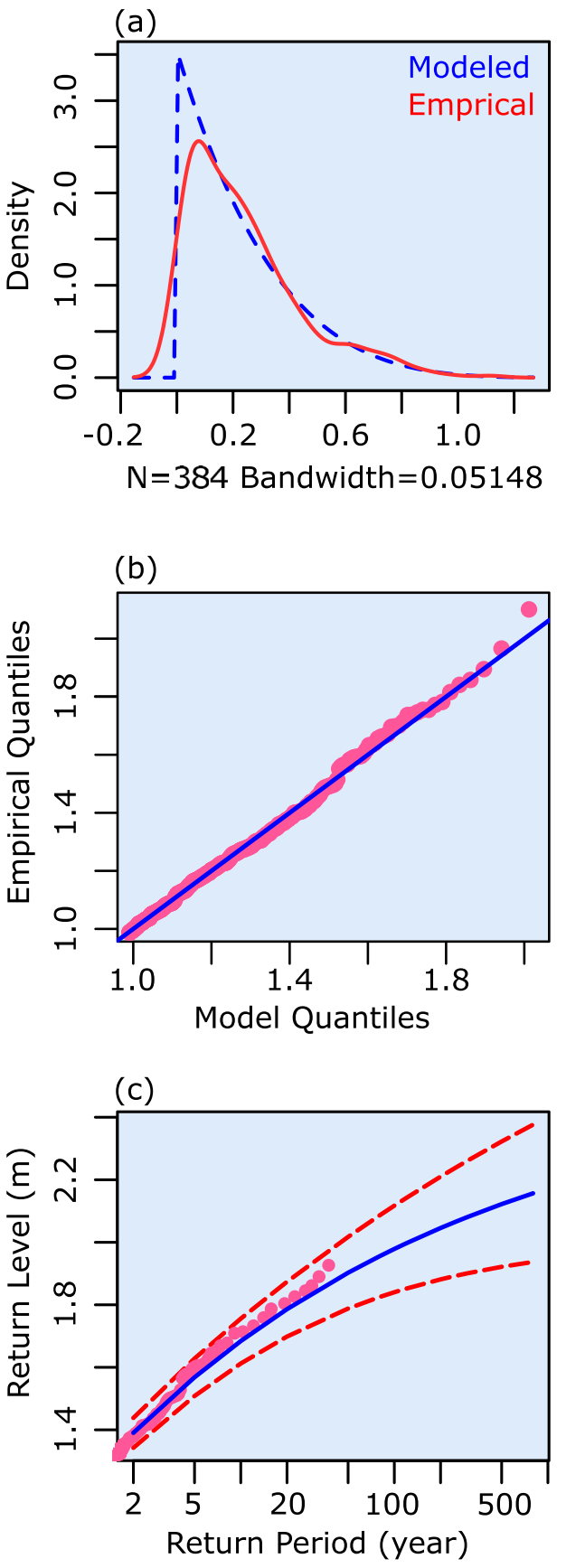

Fig. 17. Diagnostic plots from fitting the GP distribution function to independent storms (a) Density plot of empirical data and fitted GP distribution function (b) Quantile quantile plot (c) Return level plot with 95% confidence intervals.

Table 4
Return levels calculated using POT analysis (threshold = 1m, Δt = 3 days) and different parameter estimation methods.

Return period (year)	Return level (m)	
	LMoments	MLE
10	1.86	1.86
25	2.00	2.01
50	2.05	2.06
100	2.08	2.09

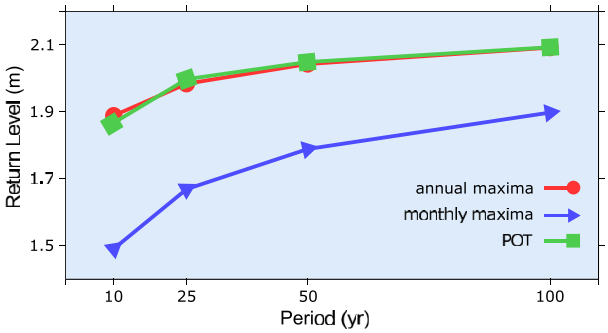

Fig. 18. Comparison of return levels determined by annual maxima, monthly maxima and POT analyses.

Table 5
Return levels for time span Δt = 3 days and various thresholds.

Return period (year)	Threshold (m) for Δt = 3 days				
	0.8	0.9	1.0	1.1	1.2
10	1.71	1.78	1.86	1.91	1.95
25	1.91	1.96	2.01	2.04	2.06
50	1.99	2.03	2.06	2.08	2.09
100	2.04	2.07	2.09	2.10	2.11

Table 6
Return levels for time span Δt = 4 days and various thresholds.

Return period (year)	Threshold (m) for Δt = 4 days				
	0.8	0.9	1.0	1.1	1.2
10	1.75	1.81	1.87	1.93	1.96
25	1.94	1.98	2.02	2.05	2.06
50	2.02	2.04	2.06	2.08	2.09
100	2.06	2.08	2.09	2.10	2.10

Table 7
Return levels for time span Δt = 5 days and various thresholds.

Return period (year)	Threshold (m) for Δt = 5 days				
	0.8	0.9	1.0	1.1	1.2
10	1.81	1.86	1.91	1.93	1.96
25	1.98	2.01	2.04	2.05	2.06
50	2.04	2.06	2.08	2.08	2.09
100	2.08	2.09	2.10	2.10	2.10

the 'mean excess', which is defined as the mean of the exceedances of u minus u. The plot should be linear above the threshold at which the GP model becomes valid. In this study, both approaches are employed to determine the threshold. Results are depicted in Fig. 14, which suggests that both scale and shape parameters show stable behavior around 1 m. Therefore, a threshold of 1 m can be considered as a suitable choice for POT analysis. The interpretation of a mean residual life plot is not always easy. As can be seen from Fig. 14b, the plots are almost linear around $u = 1$ m, and then appear to decrease sharply from $u > 1.1$ m. Therefore, a threshold of 1 m is chosen to perform POT analysis.

Table 8
Return levels for time span Δt = 6 days and various thresholds.

Return period (year)	Threshold (m) for Δt = 6 days				
	0.8	0.9	1.0	1.1	1.2
10	1.88	1.93	1.92	1.97	2.00
25	2.02	2.05	2.04	2.07	2.08
50	2.07	2.08	2.08	2.09	2.10
100	2.09	2.10	2.10	2.10	2.11

Table 9
Summary of AIC and BIC values calculated from different models using annual maxima data.

Criteria	Model				
	GEV	Weibull	Gumbel	Gamma	Log-normal
AIC	−9.89	−8.24	−8.36	−11.35	−8.91
BIC	−4.73	−5.01	−5.13	−8.13	−7.98

Mazas and Hamm (2011) showed that along with GEV and GP distribution functions, the Gamma distribution function often behaves well in terms of fitting the data. Therefore, performance of Gamma distribution function is also examined. The cumulative distribution function of Gamma is given by

$$F(z,\sigma,\xi) = \frac{\gamma(\xi, z/\sigma)}{\Gamma(\xi)} \tag{5}$$

where Γ is the Gamma function and γ is the lower incomplete gamma function.

To demonstrate and assess the performance of different extreme value analysis models, the simulated wave heights at Stingray Point are used in this section. Both GEV and POT analysis are performed. For GEV analysis, annual and monthly maxima are extracted from simulated wave height data. The parameter estimation is performed by MLE and L-moments. The results of MLE are shown in Fig. 15. The density plots (Fig. 15a,d) show good agreement between the empirical density (red line) and that of the fitted GEV distribution function (dashed blue line) for both annual and monthly maxima. Fig. 15b,e show Q-Q plots of the empirical data quantiles against those derived from the fitted GEV distribution function. The plots are reasonably straight indicating that the utilization of the GEV distribution function is fulfilled by good approximation. For annual maxima (Fig. 15b), a slight deviation from the straight line can be observed, however, this deviation is typical for extreme value analysis because of uncertainties associated with extreme value problems. Finally, Fig. 15c,f show the return levels corresponding to different return periods of extreme wave heights for annual and monthly maxima respectively. The points on the graphs (Fig. 15c,f) are the estimated return levels from annual and monthly maxima data, respectively. The solid blue lines are the estimated return levels based on the fitted GEV model and the dashed red lines are 95% confidence intervals. For both models, the empirical values fall within the 95% confidence intervals and close to the estimated return level, especially, for the monthly maxima model, showing that both models can provide acceptable values for return levels. More detailed information regarding the return levels using different parameter estimators are presented in Table 2 and Table 3, respectively. Both the plots and tables show that return levels extracted from annual maxima data have higher values compared to those extracted from monthly maxima data. For example, return levels for 10, 25, 50 and 100 years return periods from annual maxima data are 26%, 19%, 14% and 10% higher than those from monthly maxima data. It can be also seen from the tables that there are minor changes in return levels in terms of using

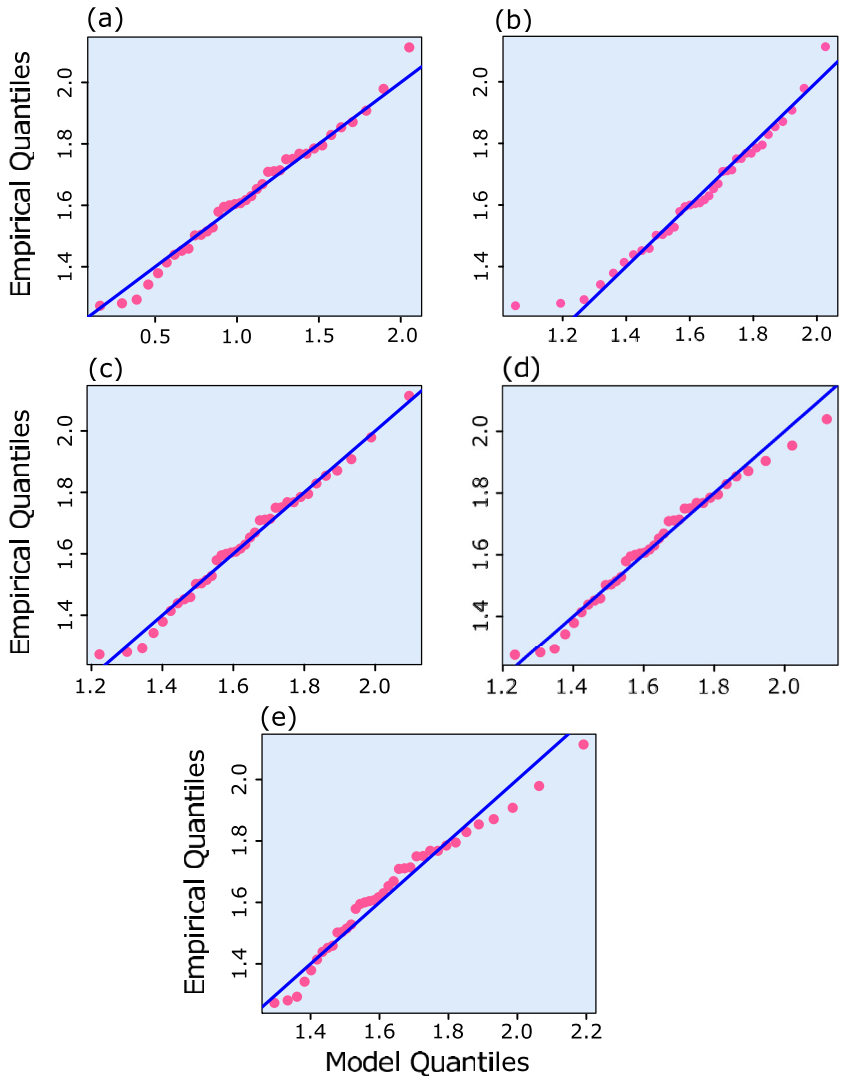

Fig. 19. Q-Q plots derived from (a) GEV (b) Weibull (c) Gamma (d) Log-normal (e) Gumbel distribution functions.

Table 10
Summary of AIC and BIC values calculated from different models using monthly maxima data.

Criteria	Model				
	GEV	Weibull	Gumbel	Gamma	Log-normal
AIC	163.52	197.43	171.66	161.82	168.06
BIC	173.81	205.63	179.86	170.01	172.25

different parameter estimators. The variation of return level is less than 0.6%, indicating that both estimators can be used for extreme value analysis of wave height.

For POT analysis, a threshold of 1 m and a time span of 3 days are selected, which results in 386 independent storms. The yearly distribution of storm events is presented in Fig. 16. It can be seen from Fig. 16a that more than 75% of storm events occur in the winter season. Fig. 16b shows the distribution of independent storms above 1m in year day, in which extreme storm events, annual maxima and 5-largest storms in each year are presented with different symbols. The largest wave heights appear in the later hurricane season (Sep. and Oct.). As detected by EOF analysis, seasonal variation of extreme wave heights is observed.

The results using MLE estimator is presented in Fig. 17. Density plot (Fig. 17a) shows a good agreement between the empirical density function (red line) and the fitted GP distribution function (dashed blue line). Similar to GEV model, Q-Q plot (Fig. 17b) from GP model is straight indicating that GP distribution function can be used for EVA with good approximation. The empirical points (Fig. 17c) are very close to the estimated return levels from GP distribution function showing that it provides good approximation for return levels. Comparisons of return levels using different estimators are shown in Table 4. Slight differences on return levels are observed using MLE and L-moments estimators.

Comparison of return levels obtained from GEV and POT show that POT and GEV produce almost the same results, especially for higher return periods. For example, for 100 year return period, POT and annual maxima GEV produce the same results, while, for monthly maxima GEV model the difference is only 10%. From the above analyses, it can be concluded that both GEV and POT are reliable approaches for estimating design wave heights. More detailed comparisons of these three approaches are presented in Fig. 18, in which return levels or design wave heights are plotted against return periods using MLE estimator. The conclusions are the same as what are observed in Tables 2–4.

5. Discussions

The choice of distribution functions, the selection of threshold and time span as well as data length included in the analysis are important in extreme value assessment. Therefore, this section is devoted to perform

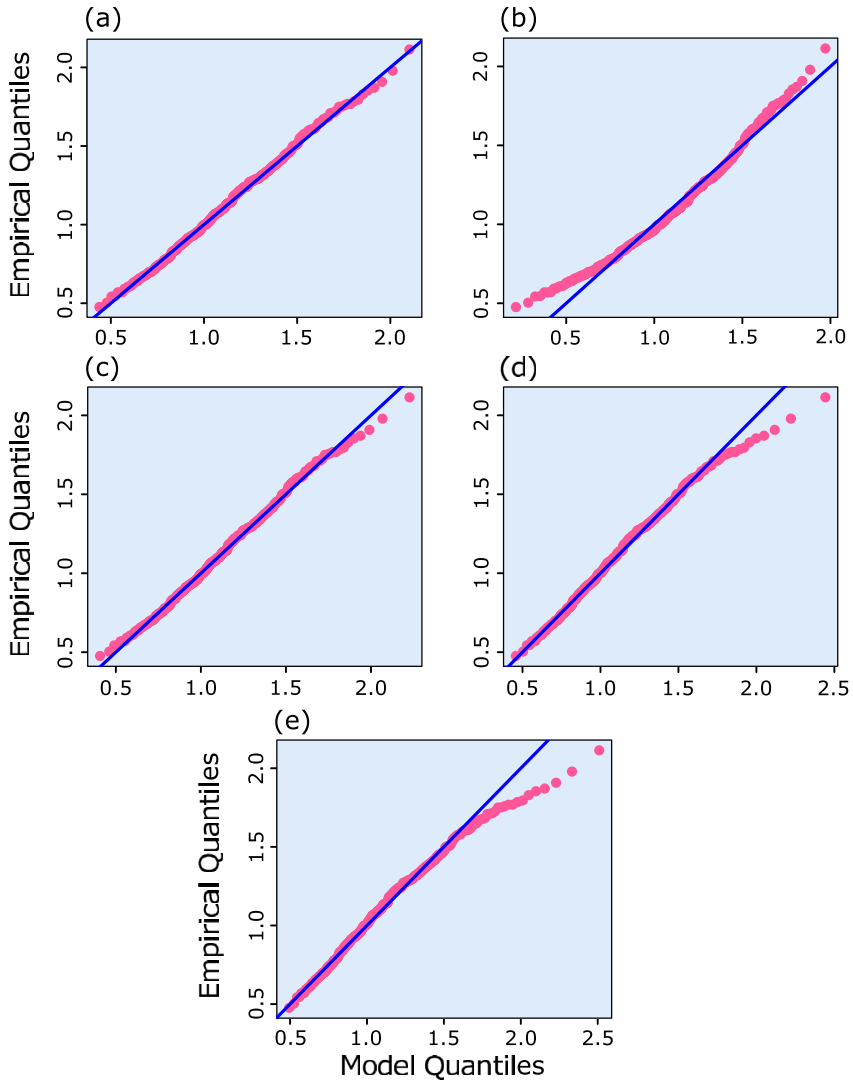

Fig. 20. Q-Q plots derived from (a) GEV (b) Weibull (c) Gamma (d) Log-normal (e) Gumbel distribution functions.

Table 11
Summary of AIC and BIC values calculated from different models using threshold of 0.8m and time span of 3 days.

Criteria	Model		
	GP	Gamma	Log-normal
AIC	−568.89	−234.31	−283.85
BIC	−559.52	−224.94	−274.48

sensitivity analyses of these parameters to understand the effects of each parameter on the estimation of design wave height.

5.1. Threshold and time span

In order to investigate the impacts of threshold wave height and time span on design wave heights, a sensitivity analysis is performed by choosing values of 0.8, 0.9, 1.0, 1.1 and 1.2 m for threshold wave height and 3, 4, 5 and 6 days for time spans. The return levels are calculated using MLE estimator and results for different time spans are shown in Tables 5–8.

It is shown that design wave height generally increases for different return periods with increasing time span. Another interesting result is that, for a specific time span, higher threshold wave height results in higher return level. Although, the variation rates of return levels are very small, especially, for higher return periods.

5.2. Distribution functions

In order to evaluate the performance of GEV and GP distribution functions in terms of fitting the data, a comparison is made between GEV distribution functions and Weibull, Gumbel, Gamma and Log-normal distribution functions by calculating Bayesian Information Criterion (BIC), also known as the Schwarz Criterion (Schwarz, 1978) and Akaike Information Criterion (AIC) (Akaike, 1974). BIC minimizes the bias between the fitted model and the unknown true model, which is given by

$$BIC = -2lnL + k_p lnN \tag{6}$$

where L is the likelihood of the fit, N is the sample size (number of storm peaks above threshold) and k_p is the number of parameters of the distribution. The AIC which can be inferred as the best compromise between bias and variance is given by

$$AIC = 2lnL + 2k_p \tag{7}$$

A lower value of AIC or BIC indicates a better fit. It is worth noting that the best fit does not necessarily provide the desirable result for design purposes, as selecting a conservative return level seems more

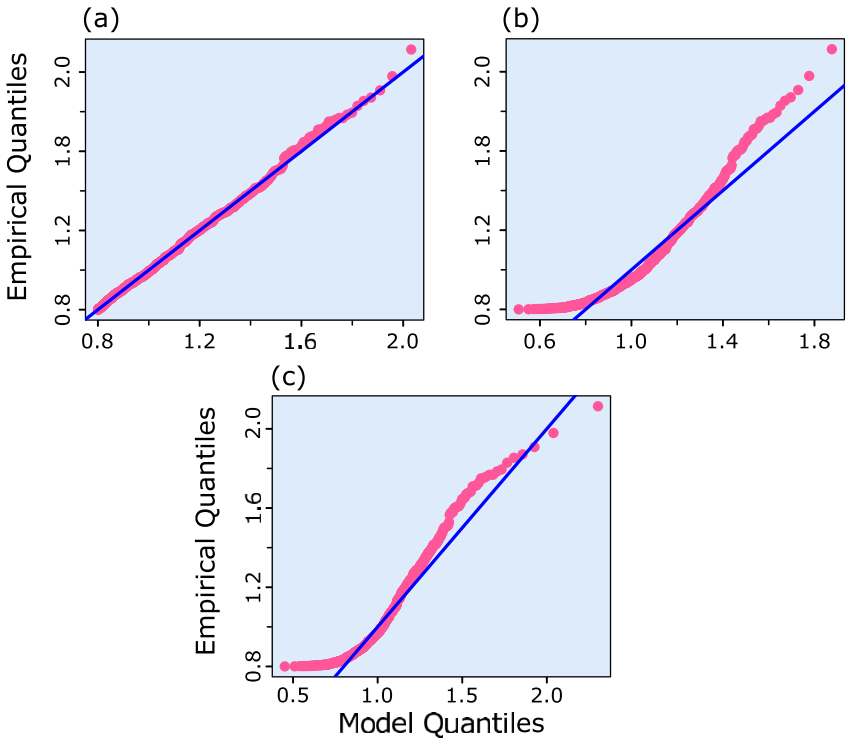

Fig. 21. Q-Q plots derived from (a) GP (b) Gamma (c) Log-normal distribution functions.

Table 12
Summary of 100-year design wave height obtained from various dataset and models.

Model	Dataset			
	1979–88	1979–97	1979–2006	1979–2015
GEV-monthly maxima	1.76	1.78	1.87	1.90
GEV-annual maxima	1.77	1.84	2.10	2.09
Gamma-monthly maxima	1.85	1.87	1.90	1.90
Gamma-annual maxima	1.91	1.96	2.09	2.12
GP (u = 1 m, Δt = 3 days)	1.90	1.96	2.06	2.09

reasonable.

The goodness of fit test is firstly performed on GEV, Weibull, Gumbel, Gamma and Log-normal using annual maxima data. Table 9 shows the summary of AIC and BIC values calculated for different models using MLE.

It can be seen from Table 9 that there is a slight difference between AIC and BIC calculated from the models showing that nearly all models are capable of fitting the annual maxima data. However, Gamma distribution function gives the best fit and GEV provides a better fit than Weibull and Gumbel distribution functions. Q-Q plot is employed to qualitatively compare the performance of all models and to check whether or not the actual and model data sets come from a population with the same distribution (Fig. 19). For Gumbel and Weibull distribution functions, Q-Q plots confirm AIC and BIC tests shown in Table 9 as some points deviate from the straight line. However, for GEV, log-normal and Gamma distribution functions, the points fall approximately along the reference line indicating that these models provide better fits.

Analyses are also performed on monthly maxima data to evaluate the performance of all models. The results are presented in Table 10.

Clearly, Weibull distribution function fails to give a good fit since AIC and BIC values of this model are much higher compared to others and Gamma distribution function still provides the best fit. Q-Q plots (Fig. 20) show graphically that Weibull and Gumbel distribution functions are not good options for EVA on extreme wave heights and GEV and Gamma distribution functions provide the best fits among all models. The Log-normal distribution function is not able to capture the tail of distribution function with deviations from the central line.

For POT analysis, GP distribution function is compared with Gamma and Log-normal distribution functions and the results of AIC and BIC tests are shown in Table 11. In this analysis, threshold wave height of 0.8 m and time span of 3 days are chosen. Q-Q plots (Fig. 21) are also drawn to verify results obtained from AIC and BIC tests. It shows that none of distribution functions are suitable for POT analysis except GP distribution function, which can be considered as a suitable tool for POT analysis of the data.

5.3. Length of data used in the analysis

The length of data included in the analysis can also play a significant role in obtaining the proper design wave height. Therefore, a sensitivity analysis is performed in terms of sample duration, by using 10, 19, 28 and 37 years datasets corresponding to the datasets during 1979–88, 1979–97, 1979–2006 and 1979–2015, respectively. The design wave heights with a return period of 100 years are obtained using GEV, Gamma and GP distribution functions.

It can be seen from Table 12 that longer dataset results in higher design wave height, which contradicts the findings of Mazas and Hamm (2011) that shorter dataset produced higher design wave height. This contradiction is mostly due to the property of data being analyzed. Since extreme events are unpredictable, higher design wave height can be obtained in smaller datasets if extreme storm events happen during that time period. In addition, a minor difference (2% maximum difference) between design wave heights obtained from 28-and 37-year dataset is obtained, suggesting that 28 years might be sufficiently long for extreme wave height analysis. The maximum difference intensifies for 10- and 19-year dataset compared to 37-year dataset by 18% and 14%, respectively. Therefore, these datasets can not provide good estimates of design wave height for 100-year return period.

Based on the analyses performed in this study, Gamma, GEV and GP distribution functions are selected to draw contours of design wave

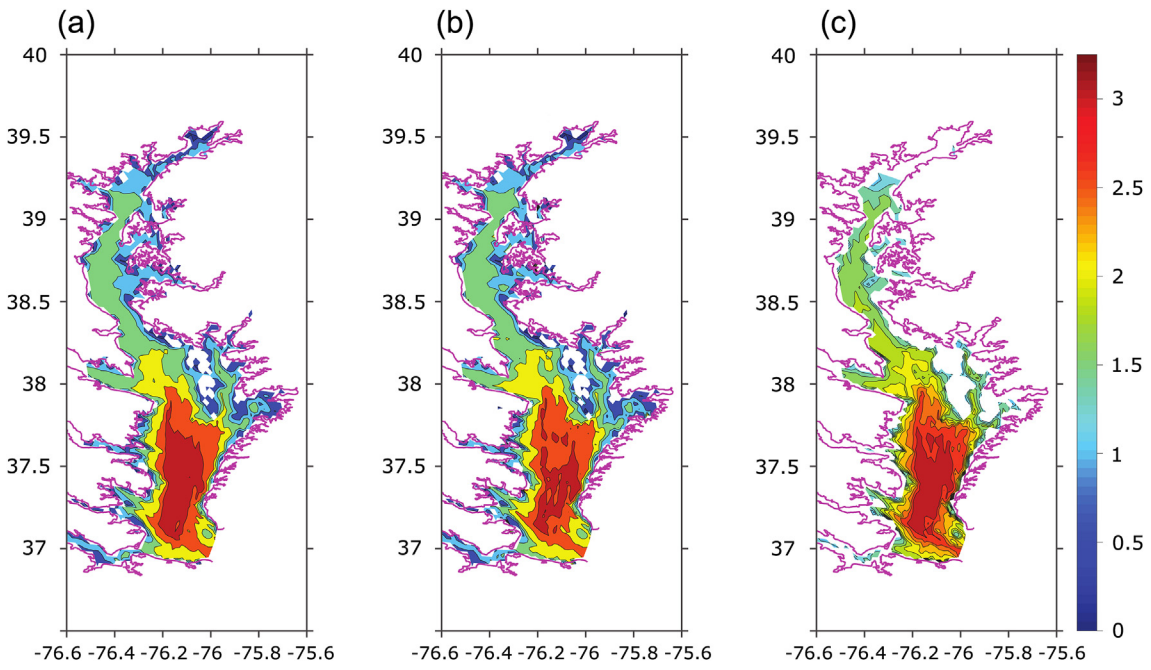

Fig. 22. Contours of design wave heights (in meters) with 100 years return period determined by using (a) Gamma (b) GEV (annual maxima) (c) GP distribution functions (u = 1m, Δt = 3 days) inside Chesapeake Bay.

heights with 100-year return period for the entire Chesapeake bay. The results are shown in Fig. 22. The design wave height generally decreases from lower bay to the upper bay, with design wave height between 1.5 and 2 m in the upper bay. It increases substantially in the lower bay and reaches up to 3.25 m. Gamma distribution function gives a more conservative estimate of design wave height (Fig. 22a) compared to GEV and GP distribution functions (Fig. 22b–c). GP distribution function fails to provide design wave height in shallow areas since its analysis is based on a threshold value that might be greater than largest waves in those areas.

6. Conclusions

In this paper, SWAN wave model was applied to reconstruct the wave climate in Chesapeake bay during 1979–2015. The spatial and temporal variabilities of the simulated wave heights in the bay were firstly analyzed using EOF analysis, regression analysis as well as cumulative distribution function analysis. EOF analysis performed on daily-averaged SWHs showed seasonal variability of wave heights in Chesapeake bay with larger wave heights in winter season. It also revealed that the lower bay experienced more significant variations in wave height. Extreme storm events such as hurricanes and tropical storms could be detected from the first mode of PC. Regression analysis on SWHs at Stingray Point suggested that there was a steady increase of extreme wave heights in the Chesapeake Bay, however, the long-term change was not significant. The continuous increase of extreme waves was further verified by empirical cumulative distribution function analysis for two separate periods: 1979–1997 and 1998–2015, in which a 9% increase in extreme wave height was observed in 99.5 percentile. These findings were confirmed by obtaining 99.5 percentile for the entire bay. Results suggested that except lower bay, where there was a maximum of 0.27m decrease in wave height, the rest of the bay received an average wave height increase of 0.1 m.

In the extreme value analysis, both GEV and POT methods were applied to estimate design wave heights. The reliability of these methods was extensively studied. The effects of key parameters such as threshold value, time span as well as data length on the design wave heights were evaluated. The GEV and POT analyses performed on annual and monthly maxima and independent extreme waves with threshold of 1.0 m and time span of 3 days showed that design wave heights with 100-year return period evaluated from GEV for annual maxima data and GP model were higher than those from monthly maxima data by 10%. Therefore, annual maxima and POT approaches provided a more conservative estimate of design wave height for design purposes. The effects of time span and threshold on design wave height were examined by tests on different time spans (3, 4, 5 and 6 days) and various thresholds (0.8, 0.9, 1, 1.1 and 1.2 m). It was found that increasing time span leaded to larger design wave height, and higher threshold resulted in higher design wave height. Moreover, sensitivity analysis on data duration showed that a 28-year dataset could provide an acceptable estimate of design wave height in the bay. The performance of GEV and GP was also evaluated in terms of fitting the data against various distribution functions including Weibull, Gumbel, Gamma, Log-normal distribution functions using AIC/BIC test and Q-Q plots. Results indicated that Gamma and GEV provided the best fit for annual and monthly data, while GP distribution function gave the best fit when POT analysis was conducted.

Acknowledgments

Ma acknowledges the financial support from PADI Foundation. Lou thanks for the support from the National Natural Science Foundation of China (NSFC 41602244).

References

Allan, J., Komar, P., 2000. Are ocean wave heights increasing in the eastern north pacific? EOS, Trans. Am. Geophys. Union 81, 561–567.
Allan, J.C., Komar, P.D., 2006. Climate controls on U.S. west coast erosion processes. J. Coast. Res. 511–529.
Akaike, H., 1974. A new look at the statistical model identification. IEEE Trans. Automat. control 19, 716–723.
Anderson, J.D., Wu, C.H., Schwab, D.J., 2015. Wave climatology in the apostle islands, lake superior. J. Geophys. Res. Oceans 120, 4869–4890.
Bacon, S., Carter, D., 1991. Wave climate changes in the north atlantic and north sea. Int. J. Climatol. 11, 545–558.
Carter, D., Draper, L., 1988. Has the north-east atlantic become rougher? Nature 332, 494.
Chawla, A., Spindler, D.M., Tolman, H.L., 2013. Validation of a thirty year wave hindcast using the climate forecast system reanalysis winds. Ocean. Model. 70, 189–206.
Coles, S., Bawa, J., Trenner, L., Dorazio, P., 2001. An Introduction to Statistical Modeling of Extreme Values. Springer.

Cooley, D., 2013. Return Periods and Return Levels under Climate Change, in: Extremes in a Changing Climate. Springer, pp. 97–114.
Cooley, D., 2009. Extreme value analysis and the study of climate change. Clim. change 97, 77–83.
Cooley, D., Nychka, D., Naveau, P., 2007. Bayesian spatial modeling of extreme precipitation return levels. J. Am. Stat. Assoc. 102, 824–840.
Farnsworth, K.L., Mary, 1997. Response Modes of the Lower Chesapeake Bay Wave Field. Ph.D. thesis. The College of William.
Graham, N.E., Diaz, H.F., 2001. Evidence for intensification of north pacific winter cyclones since 1948. Bull. Am. Meteorol. Soc. 82, 1869–1893.
Gumbel, E.J., 2012. Statistics of Extremes, Courier Corporation. Dover Publications.
Goda, Y., 1992. Uncertainty of design parameters from viewpoint of extreme statistics. J. offshore Mech. Arct. Eng. 114, 76–82.
Hawkes, P.J., Gonzalez-Marco, D., Sanchez-Arcilla, A., Prinos, P., 2008. Best practice for the estimation of extremes: a review. J. Hydraul. Res. 46, 324–332.
Katz, R.W., Parlange, M.B., Naveau, P., 2002. Statistics of extremes in hydrology. Adv. Water Resour. 25, 1287–1304.
Komar, P.D., Allan, J.C., 2007. Higher waves along us east coast linked to hurricanes. EOS, Trans. Am. Geophys. Union 88, 301.
Komar, P.D., Allan, J.C., 2008. Increasing hurricane-generated wave heights along the us east coast and their climate controls. J. Coast. Res. 479–488.
Komar, P.D., Allan, J.C., Ruggiero, P., 2009. Ocean Wave Climates: Trends and Variations Due to Earth?s Changing Climate, Handbook of Coastal and Ocean Engineering. World Scientific Publishing Co, pp. 971–975.
Kotz, S., Nadarajah, S., 2000. Extreme Value Distributions: Theory and Applications. World Scientific.
Lemke, L., Miller, J.K., 2017. EOF analysis of shoreline and beach slope variability at a feeder beach constructed within a groin field at long branch, New Jersey. Coast. Eng. 121, 14–25.
Lian, T., Chen, D., 2012. An evaluation of rotated EOF analysis and its application to tropical pacific SST variability. J. Clim. 25, 5361–5373.
Luceno, A., Menendez, M., Mendez, F.J., 2006. The effect of temporal dependence on the estimation of the frequency of extreme ocean climate events. In: Proceedings of the Royal Society of London a: Mathematical, Physical and Engineering Sciences, 462, pp. 1683–1697.
Mathiesen, M., Goda, Y., Hawkes, P.J., Mansard, E., Martin, M.J., Peltier, E., Thompson, E.F., Van Vledder, G., 1994. Recommended practice for extreme wave analysis. J. Hydraul. Res. 32, 803–814.
Martins, E.S., Stedinger, J.R., et al., 2000. Generalized maximum-likelihood generalized extreme-value quantile estimators for hydrologic data. Water Resour. Res. 36, 737–744.
Mazas, F., Hamm, L., 2011. A multi-distribution approach to pot methods for determining extreme wave heights. Coast. Eng. 58, 385–394.
Mendez, F.J., Menendez, M., Luceno, A., Losada, I.J., 2006. Estimation of the long-term variability of extreme significant wave height using a time-dependent peak over threshold (pot) model. J. Geophys. Res. Oceans 111.
Menendez, M., Mendez, F.J., Losada, I.J., Graham, N.E., 2008. Variability of extreme wave heights in the northeast pacific ocean based on buoy measurements. Geophys. Res. Lett. 35.
Mentaschi, L., Besio, G., Cassola, F., Mazzino, A., 2015. Performance evaluation of WAVEWATCH III in the mediterranean sea. Ocean. Model. 90, 82–94.
Messie, M., Chavez, F., 2011. Global modes of sea surface temperature variability in relation to regional climate indices. J. Clim. 24, 4314–4331.
Muir, L.R., El-Shaarawi, A., 1986. On the calculation of extreme wave heights: a review. Ocean. Eng. 13, 93–118.
Muraleedharan, G., Lucas, C., Soares, C.G., Nair, N.U., Kurup, P., 2012. Modelling significant wave height distributions with quantile functions for estimation of extreme wave heights. Ocean. Eng. 54, 119–131.
Rascle, N., Ardhuin, F., 2013. A global wave parameter database for geophysical applications. part 2: model validation with improved source term parameterization. Ocean. Model. 70, 174–188.
Roundy, P.E., 2015. On the interpretation of EOF analysis of ENSO, atmospheric Kelvin waves, and the MJO. J. Clim. 28, 1148–1165.
Ruggiero, P., Komar, P.D., Allan, J.C., 2010. Increasing wave heights and extreme value projections: the wave climate of the us pacific northwest. Coast. Eng. 57, 539–552.
Rusu, L., Bernardino, M., Guedes Soares, C., 2009. Influence of wind resolution on the prediction of waves generated in an estuary. J. Coast. Res. 56, 1419–1423.
Saha, S., Moorthi, S., Pan, H.-L., Wu, X., Wang, J., Nadiga, S., Tripp, P., Kistler, R., Woollen, J., Behringer, D., et al., 2010. The NCEP climate forecast system reanalysis. Bull. Am. Meteorol. Soc. 91, 1015.
Saha, S., Moorthi, S., Wu, X., Wang, J., Nadiga, S., Tripp, P., Behringer, D., Hou, Y.-T., Chuang, H.-y., Iredell, M., et al., 2014. The NCEP climate forecast system version 2. J. Clim. 27, 2185–2208.
Schwarz, G., 1978. Estimating the dimension of a model. Ann. Stat. 6, 461–464.
Stopa, J.E., Cheung, K.F., Tolman, H.L., Chawla, A., 2013. Patterns and cycles in the climate forecast system reanalysis wind and wave data. Ocean. Model. 70, 207–220.
Stopa, J.E., Cheung, K.F., 2014. Intercomparison of wind and wave data from the ECMWF reanalysis interim and the NCEP climate forecast system reanalysis. Ocean. Model. 75, 65–83.
Tasdighi, A., Arabi, M., Osmond, D.L., 2017. The relationship between land use and vulnerability to nitrogen and phosphorus pollution in an urban watershed. J. Environ. Qual. 46, 113–122.
Tolman, H.L., Banner, M.L., Kaihatu, J.M., 2013. The NOPP operational wave model improvement project. Ocean. Model. 70, 2–10.